Three-Dimensional Rarefied Flow Simulations for the Aeroassist Flight Experiment Vehicle

M. Cevdet Celenligil*
Vigyan Research Associates, Inc., Hampton, Virginia 23666
and
James N. Moss† and Robert C. Blanchard*
NASA Langley Research Center, Hampton, Virginia 23665

Hypersonic rarefied flow about the Aeroassist Flight Experiment vehicle has been investigated using a three-dimensional direct simulation Monte Carlo method. Calculations are performed for the transitional flows encountered during the vehicle's atmospheric entry for altitudes of 110 and 100 km with an entry velocity of 9.9 km/s. The simulations are performed using a five-species reacting gas model that accounts for rotational and vibrational internal energies. The solutions indicate that dissociation is important at altitudes of 110 km and below. Results are presented for surface pressures, convective heating, flowfield structure, and aerodynamic coefficient variations with altitude.

Nomenclature

A_{ref} = reference area
C_i = mass fraction of species i, ρ_i/ρ
C_D = drag coefficient
C_L = lift coefficient
C_m = pitching-moment coefficient
D_{ref} = reference length
L/D = lift-to-drag ratio
ρ = pressure
$\dot{q}$ = heat flux
s_1 = longitudinal coordinate along the surface (measured at the symmetry plane)
T = temperature
T_{tr} = translational temperature
U = velocity in x direction
X_i = mole fraction of species i
x,y,z = Cartesian coordinates
γ = specific heat ratio
η = distance along the stagnation streamline (measured from the body)
λ = mean free pitch
ρ = density

Subscripts

i = ith species
∞ = freestream

Introduction

THE design of future aeroassisted space transfer vehicles (ASTV) is focused on providing an efficient transportation capability that can transfer payloads between orbits in space. An ASTV mission includes aerobraking maneuvers through a planet's atmosphere with the help of aerodynamic forces. This process will significantly increase the vehicle's payload capacity, as compared with the case in which the maneuvers are accomplished using an all propulsive system. In order to help design a more reliable ASTV, NASA initiated the Aeroassist Flight Experiment[1] (AFE) (to be launched around 1994), which will simulate the flight of an ASTV returning from geosynchronous orbit. During this experimental flight, a subscale model vehicle will be deployed from the Space Shuttle orbiter and a solid rocket motor will propel the AFE vehicle into the Earth's upper atmosphere at a velocity of 9.9 km/s. The vehicle will undergo an aerobraking maneuver in which it will experience a velocity depletion of about 2.5 km/s, and the perigee altitude will be about 75 km. The AFE vehicle will then exit the atmosphere and achieve a low Earth orbit, where it will be retrieved by the orbiter. The flight data measurements will provide a data base that can be used to validate and improve the computer codes that are currently the primary source for the estimation of the aerothermal loads on the AFE and ASTV vehicles.

A recent investigation[2] concerning the rarefied flow encountered by the AFE vehicle between altitudes of 200 and 120 km showed that dissociation is negligible for these altitudes and that transitional effects are important even at an altitude of 200 km because the flow is not completely collisionless. In the present paper, the flow encountered at lower altitudes (110 and 100 km) is studied, and the findings are presented as a companion paper to Ref. 2.

Implementation of DSMC Method

In the present paper, the rarefied flow about the AFE vehicle is studied using the direct simulation Monte Carlo (DSME) method of Bird.[3] The DSME method has been developed as a physical model for rarefied flows; that is, for situations when the mean free path of the gas molecules may be large compared with the body size. In this scheme, the flow is simulated by some thousands of representative molecules in the computational domain, and the motion of the molecules is calculated for small time increments during which the molecular collisions and movements are uncoupled. The molecular collisions are calculated using the variable-hard-sphere (VHS) model,[4] and the Larsen-Borgnakke phenomenological model[5] is used to control the energy exchange between translational and internal modes. The chemical reactions are simulated with a five-species (O_2, N_2, O, N, and NO) nonequilibrium chemical kinetics model. For the conditions investigated in this study, radiation and ionization are negligible and are not considered.

Received March 24, 1989; revision received Jan. 3, 1989.

*Research Engineer. Member AIAA.
†Research Engineer. Associate Fellow AIAA.

In the present application, the three-dimensional computational grid consists of a network of deformed hexahedral (six-faced) cells, i.e., the four corners of a cell face may not be coplanar. This makes the generation of body-fitted grids possible, even on doubly curved surfaces. Furthermore, each cell is subdivided into tetrahedral subcells (which have four well-defined triangular faces) to enable tracking the molecules moving from one cell to another. The collision partners are selected probabilistically from the same subcells. Incidentally, in the past, the cells were divided into five tetrahedral subcells, but that scheme produces awkward shapes and erroneous results for thin cells with high aspect ratios on doubly curved surfaces. This geometrical deficiency is rectified in the present study by dividing the cells into six tetrahedral subcells.

Flowfield Geometry and Boundary Conditions

This study concentrates on the prediction of the aerothermal loads on the AFE vehicle, which is sketched in Fig. 1. The vehicle's forebody is generated by an elliptic cone that is elliptically blunted in the nose and is raked by a circular skirt at the aft end such that the base length is 4.25 m. Mathematical description of the forebody surface is given by Cheatwood et al.,[6] and their computer program has been used in the present calculations to generate the forebody surface grid. The afterbody of the vehicle consists of a hexagonal experimental carrier and a solid rocket motor whose axis is inclined at a 17-deg angle relative to the freestream. The x-y plane of the coordinate system is placed on the symmetry plane such that the origin is located on the geometric stagnation point and the x axis is parallel to the freestream velocity. According to the right-hand rule, the (+) z axis is directed out of the page in Fig. 1.

In the present study, calculations are made for the transitional flows encountered at 110- and 100-km altitudes. For both cases, calculations are performed in the forebody portion of the domain, and only half of the vehicle is considered because of the symmetry. The computational domain in front of the body starts at $x = -3.7$ m for the 110-km-altitude case and at $x = -1$ m for the 100-km-altitude calculations. For both cases, the AFE forebody surface is divided into 200 distorted rectangles with 20 divisions in the longitudinal direction and 10 divisions in the spanwise direction. The 110-km-altitude case has been computed using 2400 cells and 30,000 molecules, and the 100-km flow is simulated using 5400 cells and 68,000 molecules. The cells are generated such that each face of a cell is adjacent to only one neighboring cell.

In the simulations, atmospheric conditions[7] (for an exospheric temperature of 1200 K) listed in Table 1 are used at the freestream boundaries of the domain. The entry velocity is 9.9 km/s. The surface temperatures for 110- and 100-km altitudes are assumed to be uniformly distributed at 950 and 1500 K, respectively, which are calculated based on free-molecular radiative equilibrium heat transfer to the stagnation point. Complete thermal accommodation and diffuse reflection are assumed for the interaction of the gas molecules with the vehicle's surface.

Computational Results

After the simulations reached a stationary state, samples were taken every other time step during the calculations, and Figs. 2–13 present some of the time-averaged results based on 4000 samples. Surface pressure and heat-transfer-rate results on the forebody are shown in Figs. 2–5. Clearly, the surface pressure and heating attain their maximum values near the geometric stagnation point, have reasonably uniform distribution along the conical portion of the forebody aerobrake (as per design), and drop rapidly around the skirt. At 100-km altitude, the stagnation point surface heating is approximately one fourth of the peak heating calculation in Ref. 8 for 78-km altitude.

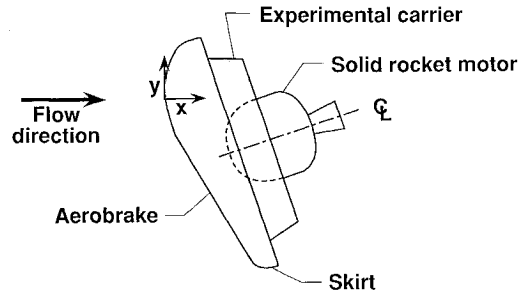

Fig. 1 AFE vehicle.

Table 1 Freestream conditions

Altitude, km	λ_∞, m	ρ_∞, kg/m^3 $\times 10^9$	T_∞, K	Mole fractions X_{O_2}	X_{N_2}	X_O
200	197.00	0.3	1026	0.031	0.455	0.514
170	75.61	0.9	892	0.044	0.548	0.408
150	30.93	2.1	733	0.055	0.616	0.330
140	16.92	3.9	625	0.062	0.652	0.286
130	7.72	8.2	500	0.071	0.691	0.238
120	2.69	22.6	368	0.085	0.733	0.183
110	0.60	96.1	247	0.123	0.770	0.106
100	0.10	558.2	194	0.177	0.784	0.039

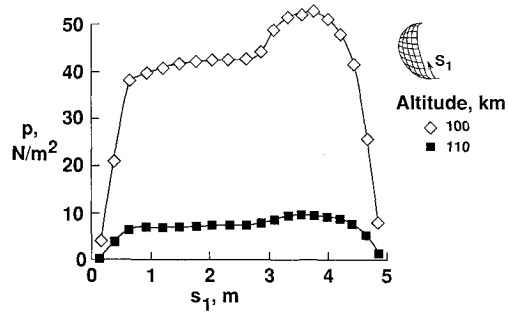

Fig. 2 Surface pressure distributions (the small sketch represents the forebody surface and grid).

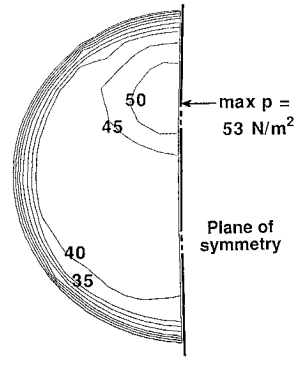

Fig. 3 Surface pressure contours (alt = 100 km).

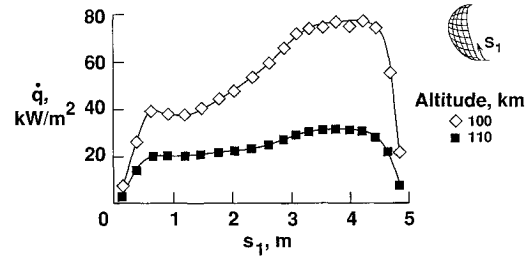

Fig. 4 Surface heat-transfer-rate distributions (the small sketch represents the forebody surface and grid).

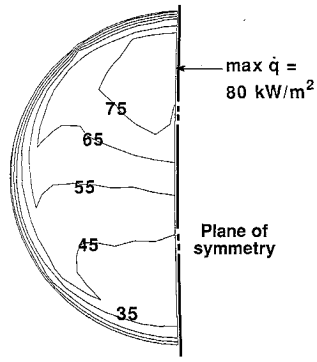

Fig. 5 Surface heat-transfer-rate contours (alt = 100 km).

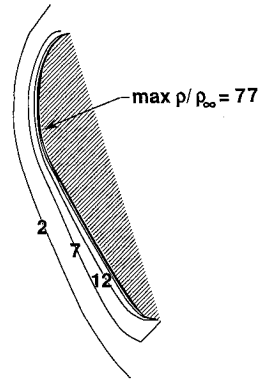

Fig. 6 Flowfield density contours at the symmetry plane (alt = 100 km).

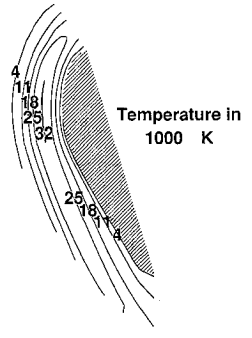

Fig. 7 Flowfield translational temperature contours at the symmetry plane (alt = 100 km).

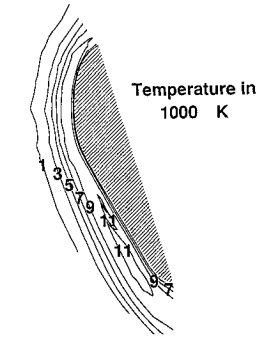

Fig. 8 Flowfield internal temperature contours at the symmetry plane (alt = 100 km).

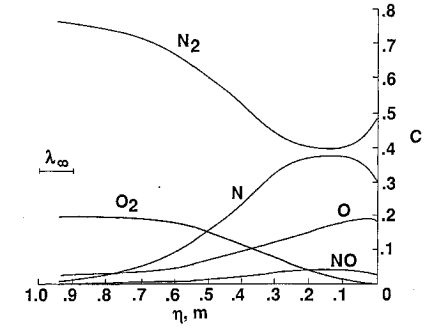

Fig. 9 Mass fraction distributions along the stagnation streamline (alt = 100 km).

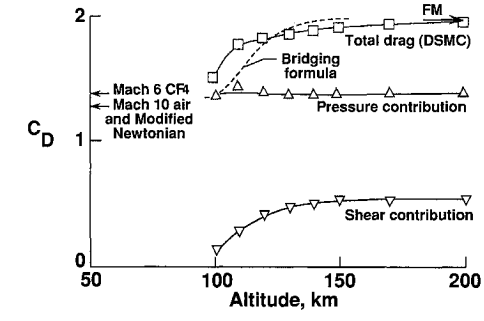

Fig. 10 Drag coefficient variation with altitude.

Figures 6–8 present some of the flowfield contours at the symmetry plane for the calculation at 100-km altitude. Figure 6 shows that the gas density increases rapidly very near the body surface. The maximum calculated value of ρ/ρ_∞ shown in Fig. 6 is an average value for the cell adjacent to the wall at the stagnation point. If smaller cells had been used, the maximum ρ/ρ_∞ value would have been > 77. (The gas density distribution adjacent to the surface is discussed in the next section.) On the other hand, as the flow approaches the vehicle, the translational (Fig. 7) and internal (Fig. 8) energies of the gas first increase and reach their peak values at some distance away from the surface, and then start decreasing because of the relatively cooler body surface. Note that the maximum translational energy occurs in front of the stagnation point, whereas the maximum internal energy occurs further downstream in the lower portion of the computational domain. This is caused by molecular collisions (during which the high kinetic energies of the molecules are converted into internal modes) experienced by the molecules as they move downstream in the lower portion of the domain. Figure 9 shows the mass fraction distributions along the stagnation streamline for the altitude of 100 km. This figure shows the effects of dissociation, which begin near 110 km as the vehicle descends in altitude.

Figures 10–13 and Table 2 show the variation of the aerodynamic coefficients with altitude. (The results of 120-km and higher altitudes are taken from Ref. 2.) Forces are normalized with respect to $\frac{1}{2}\rho_\infty U_\infty^2 A_{\text{ref}}$ and moments by $\frac{1}{2}\rho_\infty U_\infty^2 A_{\text{ref}} D_{\text{ref}}$, where ρ_∞, U_∞^2, A_{ref}, and D_{ref} are the freestream density, freestream velocity, reference area (1.41 m^2), and reference length (4.25 m), respectively. These figures and the table also contain the calculated free-molecule and modified Netwonian results along with the experimental data obtained in the NASA Langley Research Center Mach 10 air and Mach 6 CF_4 (freon) wind tunnels and documented in the AFE Aerodynamics Data Base Update II (May 1989). The CF_4 results are believed to be more appropriate as the limiting continuum values because the specific heat ratio γ for air in flight is more closely approximated in wind-tunnel tests by CF_4 ($\gamma = 1.2$) rather than by low-enthalpy air ($\gamma = 1.4$). Figures 10–12 also show the results of the Lockheed bridging formula that empirically connects the continuum and free-molecule limits. This bridging formula relies on the assumptions that continuum and free-molecule flows are established at Knudsen numbers of 0.01 and 10, respectively (which correspond to 95- and 155-km alti-

tudes in this study), and that the two limits can be connected using a sine-square function. Figures 10 and 11 also show the pressure and shear contributions on the drag and lift coefficients. Clearly, the pressure contribution is fairly constant, but the shear contribution increases with altitude such that the drag coefficient increases and the lift coefficient decreases.

One of the goals in AFE is to design the vehicle such that at hypersonic speeds the vehicle trims at zero incidence according to the coordinate system shown in Fig. 1. (This corresponds to an angle of attack of 17 deg in the AFE body axes coordinate system.) The calculated pitching-moment coefficients obtained in this study are < 0.01 (with respect to the center of gravity), but these results are grid dependent with errors comparable to the coefficient magnitude. Recently, in a separate study, the free-molecule flow aerodynamic characteristics for the AFE vehicle were investigated,[9] and it was observed by the same authors that although the drag and lift coefficients can be calculated quite accurately using only a few hundred surface cells, in order to have convergence for the pitching-moment coefficient about the center of gravity, the surface should be divided into more than 10,000 cells. To use such a surface resolution in the present study would be impractical. Therefore, the pitching moment was calculated about a point at some distance from the center of gravity such that the moment arm and, consequently, the magnitude of the pitching moment are large, and the error due to the coarse surface grid is insignificant in comparison with the magnitude of the pitching moment. In the wind-tunnel experiment, the moments were measured with respect to the center of the rake plane, which is located 2.54 m (100 in.) from the skirt of the forebody along the solid rocket motor axis; hence, this point was also chosen as the reference for C_m. The positive pitching moments shown in Fig. 13 indicate that the nose pitches downward about the (+) z axis.

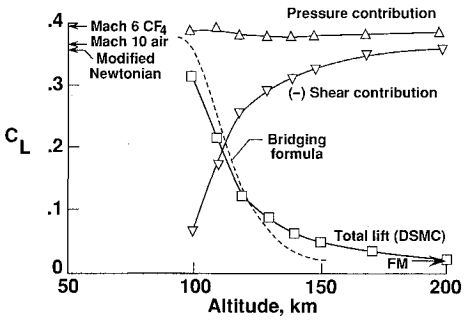

Fig. 11 Lift coefficient variation with altitude.

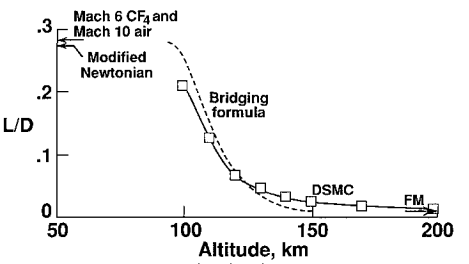

Fig. 12 Lift-to-drag ratio variation with altitude.

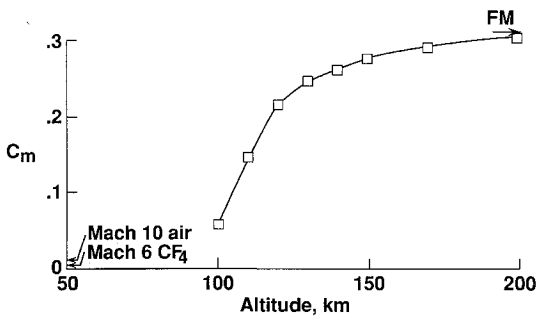

Fig. 13 Pitching-moment coefficient variation with altitude (reference located 2.54 m aft of skirt along the solid rocket motor axis).

Table 2 Aerodynamic coefficients

Altitude, km	C_D	C_L	C_m	L/D
Calculated				
(Free molecule)	1.97	0.019	0.312	0.010
200	1.95	0.025	0.303	0.013
170	1.93	0.035	0.292	0.018
150	1.90	0.049	0.278	0.025
140	1.87	0.064	0.262	0.034
130	1.84	0.086	0.248	0.046
120	1.80	0.125	0.216	0.070
110	1.71	0.218	0.146	0.128
100	1.50	0.318	0.057	0.212
(Modified Newtonian)	1.30	0.359	0.001	0.275
Experimental				
Mach 6 CF_4	1.39	0.395	0.004	0.284
Mach 10 Air	1.29	0.367	0.013	0.284

The computations were performed on the CRAY-2 at the NASA Ames Research Center. The computations for the 110-km altitude required 2M words of computer memory and 17 h of total CPU run time, whereas the 100-km-altitude computations were done using 3.5M words of memory and 35 h of computational time.

Discussion

Interpretation of the AFE vehicle's flight measurement data for the aerodynamic coefficients requires an understanding of the flow about the vehicle in a rarefied flow regime.[10] This paper concentrates on the transitional flow about the AFE vehicle during its entry into the atmosphere. The focus of the present investigation is at the 110- and 100-km altitudes, conditions at which the chemical dissociation significantly impacts the flowfield structure. In this section, before discussing the present results, a brief discussion of the past simulation efforts is given, as they relate to the current work.

The first problem investigated at the outset of this study was the case where the AFE vehicle is represented by an idealized axisymmetric geometry. This case was studied previously using an axisymmetric DSMC code between altitudes of 90 and 130 km.[11] The reason for applying the three-dimensional program to this simpler problem was to check if the three-dimensional program would reproduce the axisymmetric results before applying it to more complicated configurations. Note that for this problem, the basic computational parameters (e.g., cell sizes and time steps) were already available from the axisymmetric computations, and this eliminated the iterative process otherwise required for their determination. The initial application of the three-dimensional program concentrated on the axisymmetric flow problem at 130 km because higher altitude flows, in general, require less computational time. The calculated three-dimensional results were in very good agreement with those of the axisymmetric code computations. The grid used in the three-dimensional computations (8 divisions along the surface and 16 divisions in the normal direction) was coarser than the one used in the axisymmetric program (20 divisions along the surface and 40 divisions in the normal direction), and the cell structuring was different. Agreement of these results, consequently, is an indication of grid independency for the computations. For this case, the extent of the computational domain was also checked. The results showed almost no difference when the domain was started 5 m in front of the body (where density ratio $\rho/\rho_\infty = 1.5$ and translational temperature $T_{tr} = 17{,}000$ K) instead of 15 m (where $\rho/\rho_\infty = 1.0$ and $T_{tr} = 1{,}500$ K).

Subsequently, the program was applied to the three-dimensional flow about the actual AFE vehicle between altitudes of 200 and 120 km.[2] Computations for the 120- and 130-km altitudes have been used to check afterbody effects. In these computations, the base of the vehicle is the experimental carrier because the solid rocket motor is ejected during entry near 130-km altitude. The results indicate that the afterbody effects are negligible, and, consequently, for the 140-km and higher altitudes, only the forebody domain was considered. Also, the grid independency of the results for the 120-km and higher altitudes is verified.

In the present study, the calculations have been made at lower altitude conditions, namely, 110 and 100 km. The computational requirements, in terms of computing time, for the DSMC method increase substantially with increasing gas density, and, therefore, the lowest altitude investigated in this study is 100 km. In order to reduce the computation time, only the forebody domain is considered for both the 110- and 100-km cases, assuming that the afterbody effects are not significant. This assumption is reasonable because calculations for Project Fire (which is also a blunt body like the AFE vehicle) have shown that the afterbody influence is minimal,[12] even for lower Knudsen number conditions when compared with those of the present study. In the present study, only one computation has been performed for each of the two altitude cases. Nevertheless, in the computations, the basic DSMC requirements are satisfied. Namely, the cell sizes in the direction normal to the body are smaller than the local mean free path (the gradients in this direction are much steeper than those in the other directions), the number of molecules in each cell is of order 10, and the time step used to move the molecules is smaller than the mean collision time. Past experience indicates that the results will not differ if finer grids are used.

Comparing the present results with those at the higher altitudes[2] shows that, as the altitude decreases, significant differences are observed in the flow structure. First, the present results indicate that dissociation exists at 110 km and its effects are even more pronounced at 100 km (Fig. 9). For example, at 100-km altitude, the average molecular weight of the gas near the vehicle's forebody surface is about 30% smaller than that at the freestream; whereas at 120 km, they were almost equal.

Second, the nonequilibrium among the entry modes decreases substantially with decreasing altitude. At 120-km and higher altitudes, distinct classes of molecules are present in the flowfield, namely, freestream molecules, surface-reflected molecules, and the ones that have undergone molecular collisions. Mixing these classes of molecules produces a highly nonequilibrium flow structure because their distribution functions are widely separated in velocity space.[2] For example, for the 120-km case, the maximum translational temperature is about 10 times the maximum internal temperature in the forebody portion of the domain. As the altitude decreases, the intermolecular collisions begin to dominate the flowfield structure and the nonequilibrium among the energy modes decreases. For example, for the 100-km case, the maximum translational temperature (Fig. 7) is about three times larger than the maximum internal temperature (Fig. 8). Note that the extent of the disturbance field in front of the body also decreases substantially with decreasing altitude. For instance, the disturbance field in front of the vehicle decreases by a factor of about five as the altitude is decreased from 120 to 100 km.

Third, the computational results show an interesting feature concerning the near-surface gas density along the vehicle's forebody and its variation with altitude. Computations for altitudes from 200 to 100 km indicate that, as the flow moves downstream of the stagnation point along the lower portion of the surface,the near-surface density first decreases (along the elliptic nose), then increases (along the long and reasonably flat portion of the aerobrake), and finally drops quickly (as the flow expands around the bottom skirt). Note that this phenomenon does not occur in the upper portion of the AFE vehicle because the body surface is much shorter and is curved; hence, the density drops continuously as the flow expands around the upper surface. For the 100-km and higher altitudes, the density increase along the nearly flat section of the forebody gives rise to densities that are actually greater than the corresponding stagnation value. But as the altitude decreases to 100 km, the maximum density occurs at the stagnation point. The near-surface density rise along the lower portion of the vehicle explained earlier is also observed in separate lower altitude (90 and 75 km) AFE calculations.[13] In those calculations, the peak densities are also observed at the stagnation point.

The behavior of the density (adjacent to the surface) as the flow moves downstream of the stagnation point has also been observed for the calculated flow about a delta wing,[14] the two-dimensional flow about a finite flat plate at incidence,[15] and in Ref. 16. The flat-plate results show that, as the freestream conditions change from the free-molecular limit to a Knudsen number of about 0.02 (based on plate length), the density distribution along the plate changes from a uniform distribution to one in which the gas density increases in the downstream direction and maximum gas density occurs near the trailing edge (not at the stagnation point).

Summary

In this study, the three-dimensional rarefied flows about the AFE vehicle for altitudes of 110 and 100 km have been studied using the DSMC technique. The computational results of this study when compared with those for higher altitudes show that dissociation is important at 110-km and lower altitudes. Nonequilibrium among the energy modes is evident in the results, although this effect decreases with decreasing altitude. At 100-km altitude, maximum near-surface density occurs at the stagnation point, whereas at higher altitudes, the density reaches its maximum further downstream of the stagnation point. At 100-km and higher altitudes, surface heating is primarily caused by the convective heat transfer, and the results for these altitudes indicate that maximum surface heating and surface pressure occur near the geometric stagnation point of the vehicle.

Of course, peak surface heating occurs near the perigee of the vehicle's trajectory. But in the present study, altitudes lower than 100 km are not investigated because of their excessive computational time requirements. At 100-km altitude, the surface heating at the stagnation point is about one fourth of the peak heating at 78-km altitude. Nevertheless, the present study represents the first time that a general three-dimensional DSMC code has been used to describe the flow about a full-scale space vehicle and shows the applicability of the DSMC method to complicate three-dimensional configurations. Results such as these have important implications for the interpretation of aerodynamic coefficients extracted from flight measurements under rarefied conditions.

Acknowledgments

The authors wish to thank Frank Brock for his comments, Joseph Price for his help in generating contour plots, and Neil Cheatwood for the use of his computer program in generating the forebody surface grid.

References

[1]Walberg, G. D., Siemers, P. M., III, Calloway, R. L., and Jones, J. J., "The Aeroassist Flight Experiment," International Astronautical Federation, Paper IAF-87-197, Oct. 1987.

[2]Celenligil, M. C., Moss, J. N., and Bird, G. A., "Direct Simulatin of Three-Dimensional Flow About the AFE Vehicle at High Altitudes," *AIAA Progress in Astronautics and Aeronautics: Rarefied Gas Dynamics: Theoretical and Computational Techniques,* Vol. 118, edited by E. P. Muntz, D. P. Weaver, and D. H. Campbell, AIAA, Washington, DC, 1989, pp. 447–461.

[3]Bird, G. A., *Molecular Gas Dynamics,* Clarendon, Oxford, 1976.

[4]Bird, G. A., "Monte-Carlo Simulation in an Engineering Context," *AIAA Progress in Astronautics and Aeronautics: Rarefied Gas Dynamics,* Vol. 74, Pt. 1, edited by S. S. Fisher, AIAA, New York, 1981, pp. 239–255.

[5]Borgnakke, C., and Larsen, P. S., "Statistical Collision Model for Monte Carlo Simulation of Polyatomic Gas Mixture," *Journal of Computational Physics,* Vol. 18, No. 4, 1975, pp. 405–420.

[6]Cheatwood, M. F., DeJarnette, F. R., and Hamilton, H. H., II, "Geometrical Description for a Proposed Aeroassist Flight Experiment Vehicle," NASA TM-87714, July 1986.

[7]Jacchia, L. G., "Thermospheric Temperature, Density, and Composition: New Models," Smithsonian Astrophysical Observatory, Cambridge, MA, Special Rept. 375, March 1977.

[8]Gupta, R. N., and Simmonds, A. L., "Stagnation Flowfield Analysis for an Aeroassist Flight Experiment Vehicle," AIAA Paper 88-2613, June 1988.

[9]Blanchard, R. C., and Hinson, E. W., "Free-Molecule-Flow Force and Moment Coefficients of the Aeroassist Flight Experiment Vehicle," NASA TM-101600, July 1989.

[10]Blanchard, R. C., "Rarefied-Flow Aerodynamics Measurement Experiment on the Aeroassist Flight Experiment," AIAA Paper 89-0636, Jan. 1989.

[11]Dogra, V. K., Moss, J. N., and Simmonds, A. L., "Direct Simulation of Aerothermal Loads for an Aeroassist Flight Experiment Vehicle," AIAA Paper 87-1546, June 1987.

[12]Olynick, D. P., Moss, J. N., and Hassan, H. A., "Influence of Afterbodies on AOTV Flows," AIAA Paper 89-0311, Jan. 1989.

[13]Gnoff, P. A., "A Code Calibration Program in Support of the Aeroassist Flight Experiment," AIAA Paper 89-1673, June 1989.

[14]Celenligil, M. C., and Moss, J. N., "Direct Simulation of Hypersonic Rarefied Flow About a Delta Wing," AIAA Paper 90-0143, Jan. 1990.

[15]Dogra, V. K., Moss, J. N., and Price, J. M., "Rarefied Flow Past a Flat Plate at Incidence," *AIAA Progress in Astronautics and Aeronautics: Rarefied Gas Dynamics: Theoretical and Computational Techniques,* Vol. 118, edited by E. P. Muntz, D. P. Weaver, and D. H. Campbell, AIAA, Washington, DC, 1989, pp. 567–581.

[16]Brewer, E. B., NASA Marshall Space Flight Center, ED32, Alabama 35812, unpublished work on the three-dimensional DSMC calculations for the AFE vehicle (personal communication).